



A versatile optode system for oxygen, carbon dioxide, and pH measurements in seawater with integrated battery and logger

Christoph Staudinger,¹ Martin Strobl,¹ Jan P. Fischer,² Roland Thar,² Torsten Mayr,¹ Daniel Aigner,¹ Bernhard J. Müller,¹ Bernhard Müller,¹ Philipp Lehner,¹ Günter Mistlberger,¹ Eva Fritzsche,¹ Josef Ehartner,¹ Peter W. Zach,¹ Jennifer S. Clarke,³ Felix Geißler,³ André Mutzberg,³ Jens D. Müller ⁴, Eric P. Achterberg,³ Sergey M. Borisov ¹,* Ingo Klimant¹

¹Institute of Analytical Chemistry and Food Chemistry, Graz University of Technology, Graz, Austria

²Pyro Science GmbH, Aachen, Germany

³GEOMAR Helmholtz Centre for Ocean Research, Kiel, Germany

⁴Department of Marine Chemistry, Leibniz Institute for Baltic Sea Research Warnemünde, Rostock, Germany

Abstract

Herein, we present a small and versatile optode system with integrated battery and logger for monitoring of O₂, pH, and pCO₂ in seawater. Three sensing materials designed for seawater measurements are optimized with respect to dynamic measurement range and long-term stability. The spectral properties of the sensing materials were tailored to be compatible with a commercially available laboratory oxygen logger that was fitted into a pressure housing. Interchangeable sensor caps with appropriate “sensing chemistry” are conveniently attached to the end of the optical fiber. This approach allows using the same instrument for multiple analytes, which offers great flexibility and minimizes hardware costs. Applications of the new optode system were demonstrated by recording depth profiles for the three parameters during a research cruise in the Baltic Sea and by measuring surface water transects of pH. The optode was furthermore used to monitor the concentration of dissolved oxygen in a seagrass meadow in the Limfjord, Denmark, and sensor packages consisting of pO₂, pH, and pCO₂ were deployed in the harbors of Kiel, Germany, and Southampton, England, for 6 d. The measurements revealed that the system can resolve typical patterns in seawater chemistry related to spatial heterogeneities as well as temporal changes caused by biological and tidal activity.

Oxygen, pH, and pCO₂ are important parameters in marine science (Dickson 1984; Millero 1995; Doney et al. 2009; Millero et al. 2009; Larsen et al. 2016). All three parameters are useful to characterize water masses and are excellent indicators for many biological processes (Orr et al. 2005). Furthermore, simultaneous measurement of pH and pCO₂ is sufficient, although not ideal, for a complete characterization of the carbonate system (Millero 2007). Since the increasing atmospheric carbon dioxide (CO₂) concentrations result in ocean acidification (Caldeira and Wickett 2003; Doney et al. 2009), pH and pCO₂ measurements are of increasing interest to study the influence of this ongoing process on marine life.

*Correspondence: sergey.borisov@tugraz.at

Additional Supporting Information may be found in the online version of this article.

This is an open access article under the terms of the Creative Commons Attribution License, which permits use, distribution and reproduction in any medium, provided the original work is properly cited.

Despite the fact that many methods are available for the measurement of these parameters, only some of them are suitable for in situ monitoring. Oxygen sensors are widely used for oceanographic applications and are either electrochemical (Clark electrode) or optical (luminescent sensors). However, in situ pH measurements are more challenging. For instance, the classical pH glass electrode is not suitable for long-term measurements in high-salinity water due to ionic strength induced liquid junction potentials, which result in unstable and inaccurate results (Dickson 1984, 1993; Covington and Whitfield 2009). In recent years, ion selective field effect transistors (ISFET)-based systems have received increasing attention as an alternative to glass electrodes (Martz et al. 2010; Bresnahan et al. 2014; Takeshita et al. 2014; Johnson et al. 2016). However, they still face obstacles such as stability of the reference electrode, pressure cross-talk, and light cross-talk (Le Bris and Birot 1997; Jimenez-Jorquera et al. 2009; Martz et al. 2010; Bresnahan et al. 2014; Johnson et al. 2016). Another popular method is spectrophotometric measurements. Here, the pH dependent absorption spectrum of an

indicator dye (most commonly m-cresol purple) is measured (Byrne and Breland 1989; Clayton and Byrne 1993). These systems offer very high accuracy and precision as well as low drift, and they are used routinely for reference measurements in the laboratory. However, they require reservoirs for the indicator and the waste, as well as appropriate fluidic components such as pumps and valves. Therefore, spectrophotometric systems are comparably bulky and expensive, have dramatically increased power consumption (e.g., 6.5 W; Liu et al. 2006) and operate usually with low sampling rate. Despite these challenges, major advances in recent years made it possible to build autonomous miniaturized spectrophotometric pH sensing systems (Rérolle et al. 2012, 2013; Perez de Vargas Sansalvador et al. 2016).

A promising alternative to these methods are pH optodes, which have received increasing attention in the last few years (Clarke et al. 2015). Similarly to spectrophotometric systems, pH optodes require no potentially unstable reference electrode, they are much easier to miniaturize and are more cost-effective compared to ISFET and spectrophotometric devices. Advantageously, they do not require moving parts or reagents.

Several different sensor schemes have been developed to measure carbon dioxide in seawater. A large number of carbon dioxide sensors for oceanography are based on IR-spectroscopy (Friederich et al. 1995; Fiedler et al. 2013; Fietzek et al. 2014; Jiang et al. 2014; Sutton et al. 2014; Hunt et al. 2017). These sensors are based on the diffusion of carbon dioxide through a semi-permeable membrane into an internal gas phase and quantification of the analyte via IR absorption. Such sensor systems deliver precise and high resolution data. However, carbon dioxide sensors based on IR-spectroscopy require high power input (e.g., 0.5–7 W) (Fietzek et al. 2014; Clarke et al. 2017), regular drift corrections and they are typically bulky.

In a wet-chemical approach, the pH change of a solution induced by carbon dioxide, is recorded spectrophotometrically (Lefèvre et al. 1993; DeGrandpre et al. 1995; Lu et al. 2008).

Since carbon dioxide has to diffuse through a membrane and dissolve in the aqueous solution of the indicator, the response times are long ($t_{63} \geq 2$ min; Clarke et al. 2017). Other limitations of the spectrophotometric carbon dioxide sensors include membrane deterioration, light source instabilities, and battery lifetime (DeGrandpre et al. 1999; Lu et al. 2008; Clarke et al. 2017).

Electrochemical carbon dioxide sensors (which rely on the pH electrode as a transducer) have also been evaluated for oceanographic measurements (Severinghaus and Bradley 1958; Shitashima 2010; Xie and Bakker 2013). However, they suffer the same drawbacks as pH glass electrodes. As for pH measurements, optodes represent a promising alternative for carbon dioxide measurements (Amao and Nakamura 2004; Schutting et al. 2013, 2014, 2015; Atamanchuk et al. 2014; Clarke et al. 2017; Fritzsche et al. 2017).

Optodes usually consist of two main components: a read-out device and a luminescent or colorimetric sensing material. The optodes utilize the analyte-dependent change in the optical properties of this sensing material, most commonly luminescence lifetime (in case of oxygen optodes), fluorescence intensity, or absorption/reflectance for other analytes. This change in optical properties is quantified by the read-out device. Optodes enable remote read-out, are easy to miniaturize, have low power consumption (0.5 mW, optode with logger, 30 s measurement interval, presented in this work), and are not influenced by electromagnetic interferences. Due to these advantages, optodes are highly promising for application in numerous fields of science and technology.

While O₂ optodes are already widely used in oceanography (e.g., Aanderaa Data instruments AS, Sea & Sun Technology GmbH, Sea-Bird Scientific), pH and CO₂ optodes are at a lower Technology Readiness Level, with a lack of specialized readout devices and dedicated sensing materials limiting more widespread application. Further development will enable reliable and cost-effective measurement of both pH and pCO₂. Herein, we address this challenge and present a new versatile optode system, which enables autonomous measurements of oxygen, pH, or carbon dioxide in seawater.

Materials and procedures

Optode sensor system

The optode sensor system (Fig. 1) includes two essential components: the read-out device and the sensing material covering the top of the screw-on sensor cap. The read-out device is designed to enable autonomous long-term measurement and includes an internal Li-polymer battery and a logger in addition to the optoelectronic part. A cost-effective polyoxymethylene (POM) pressure housing is used to enable deployments down to 500 m water depth.

Read-out device

The optoelectronic unit of the optode is based on a modified version of the commercially available laboratory and field oxygen meter FireSting GO2 (PyroScience GmbH). The device utilizes a 625 nm LED for excitation, a shortpass excitation filter and a longpass emission filter to eliminate the influence of the excitation light on the photodetector. The optoelectronic unit is essentially a compact phase fluorimeter. The luminescence phase shift delivers analytical information for all parameters and is either used directly to calculate the luminescence decay time of the oxygen indicator, or to access the luminescence intensity ratio (indicator/reference) in the case of pH and pCO₂ sensors, according to the so called Dual Lifetime Referencing (DLR; Klimant et al. 2001) scheme. Modulation frequencies between 2 kHz and 4 kHz are optimal for all the sensing materials used in this work.

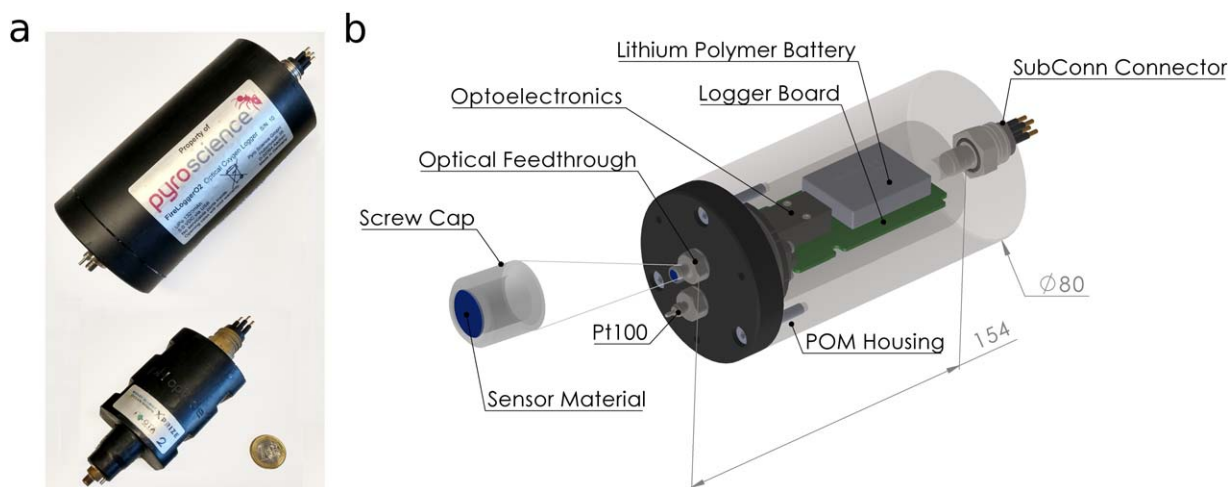


Fig. 1. (a) Photographic images of the optodes with a 1 Euro coin for size comparison. Optode in a POM housing for measurements at up to 500 m water depth (upper image) and the optode molded in polyurethane for shallow water measurements (lower image). (b) Sketch of the optode in a pressure housing with logic boards, Li-Polymer battery, optical feedthrough, temperature feedthrough, Subconn[®] connector, and screw-able sensor cap.

The optode is contained in a POM housing with a wall thickness of 15 mm, which enables an operation depth down to 500 m. An optical feedthrough with a fiber thickness of 2 mm and a theoretical pressure resistance to 3000 m is used to connect optical sensing materials. The outer end of the feedthrough is equipped with an M6x0.75 outer thread. This is used to mount the sensing materials, which are glued onto transparent poly(methyl methacrylate) caps with the respective internal thread.

Another feedthrough is implemented for a Pt-100 resistance thermometer. The temperature data are especially useful for internal temperature compensation of the sensing materials. A 6-pin Subconn[®] connector is used for power supply and communication. The choice of POM instead of titanium as housing material results in a very cost-effective and lightweight device for shallow water operations. The optode is 154 mm long, has a diameter of 80 mm and weighs 970 g in air and 200 g in water. The small size and low weight in water significantly simplifies integration into floats, as only little additional buoyancy is required. The main drawback of the POM housing is the limited operation depth of 500 m. However, this is sufficient for many coastal applications and for example the entire Baltic Sea. In these areas, the low-pressure deployment limit is not an issue and the cost-effective build enables more widespread monitoring at constant costs. The estimated hardware costs are in the range of 1000 Euro per device. For other applications, e.g., profiling in the open ocean, a conventional titanium housing could be readily designed but with increased manufacturing costs.

Autonomous measurements and long-term deployments are possible due to an internal Li-Polymer battery (1320 mAh) and logger. Due to a highly optimized power consumption of the optode and the logger, this battery capacity

is sufficient for approximately 1.4 million single measurement points, which is equivalent to a deployment time of more than 1 yr with a measurement interval of 30 s. The internal logger is able to trigger periodic measurements between 1 s and 1 h and features an internal flash memory with a storage capacity sufficient for approximately 20 million data points. Hence, both battery and storage capacity are more than sufficient for typical servicing periods of buoys and other measurement stations. Device configuration and data readout is performed via USB port using the standard Windows-based software of the device.

A second version of the device was developed for shallow water measurements up to 100 m water depth (Fig. 1a, bottom). In this device, the components of the optode are molded directly in polyurethane. This construction is in principle even more cost-effective as no machined housing is required. A casting mold was prepared from silicone rubber with a stereolithographically 3D printed positive of the device. This resulted in a very compact design and enabled the inclusion of structural features such as grooves for simple and fast mounting. In this version, a 5-pin SubConn[®] connector was used, instead of the 6-pin connector used for the device with a pressure housing.

Sensor caps

The sensing materials are mounted with a screw-cap system (Fig. 1) on an optical feedthrough. Thereby, the “sensing chemistry” (and hence the analyte of the optode) is easily exchangeable. All three sensing materials are coated onto a transparent and mechanically stable polyester support. The individual spots (5 mm diameter) are stamped out and glued onto the sensing cap.

The three sensing materials are selected to enable shared optoelectronics of the read-out device such that no exchange

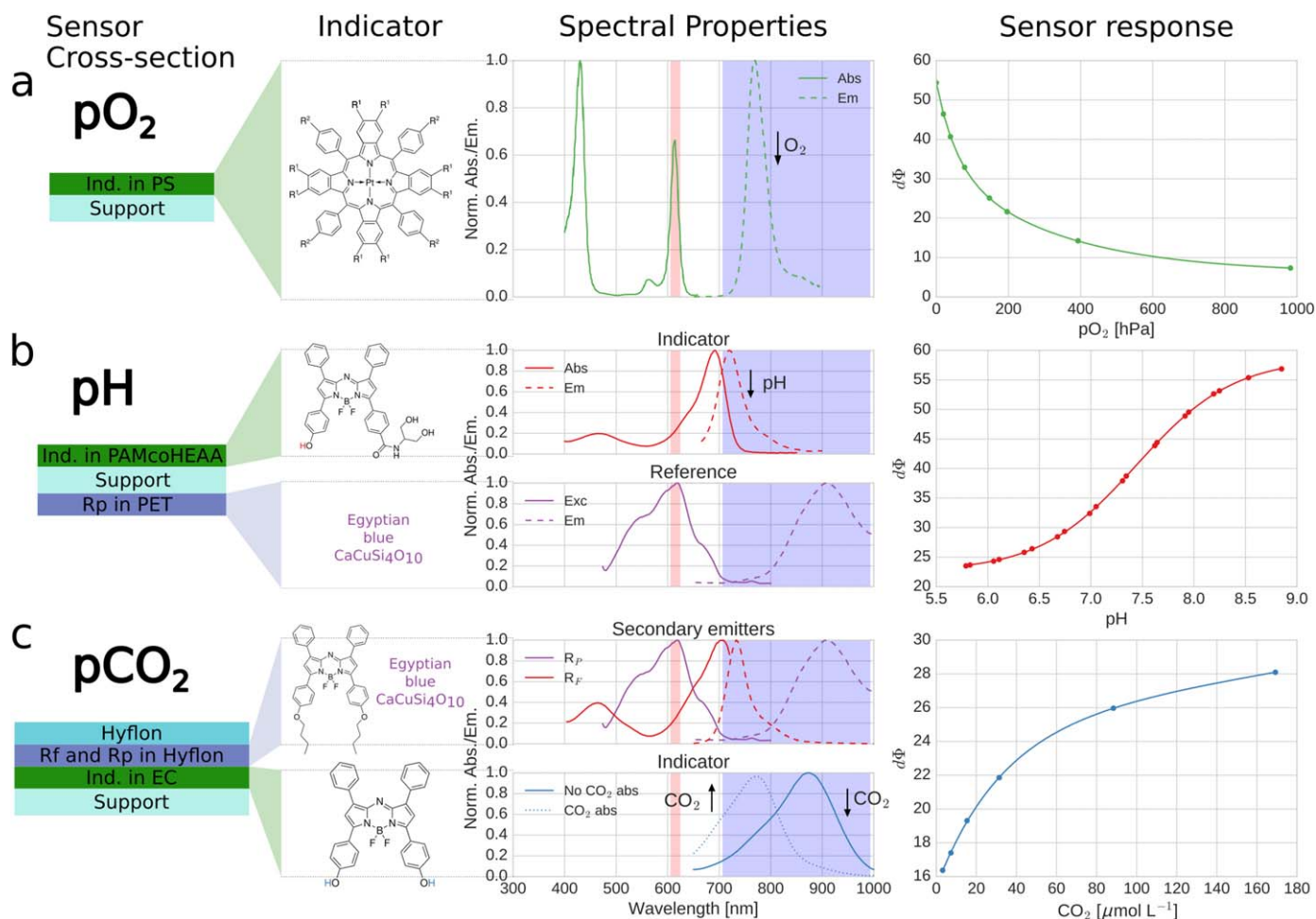


Fig. 2. From left to right: Cross-section of the sensing materials: pO₂ (a), pH (b) and pCO₂ (c); chemical structures of the indicators and the reference materials; absorption/excitation and emission spectra of the utilized dyes and phosphors; examples of calibration curves. The red and blue areas in the spectra indicate the excitation and signal collection wavelengths, respectively. Calibration curves were recorded at 10°C and at salinity 10. Ind = indicator, PS = polystyrene, PAMcoHEAA = copolymer of acryloylmorpholine and hydroxy ethyl acrylamide, Rf = fluorescent reference (dibutoxy aza-BODIPY), Rp = phosphorescent reference (Egyptian blue), EC = ethyl cellulose.

of excitation source or optical filters is necessary. The dyes are excitable with red light and emit in the near infrared part of the spectrum (Fig. 2). Since measurement of luminescence intensity is unreliable and is affected by numerous parameters, referenced readout is used for all the sensing materials. Luminescence phase shift measured by the optoelectronic unit provides the analytical information.

The pO₂ sensing material utilize a platinum(II) benzoporphyrin as an indicator dye immobilized in a polystyrene matrix (Carraway et al. 1991; Lehner et al. 2015). The utilized oxygen-sensing material was obtained from PyroScience GmbH. Importantly, this sensing material can be substituted by a trace oxygen sensor also available from PyroScience GmbH or by trace and ultra-trace sensing materials published previously, which rely on benzoporphyrins immobilized in highly gas-permeable, amorphous perfluorinated polymers (Lehner et al. 2015; Larsen et al. 2016). Since all these oxygen indicators show long-lived

phosphorescence, the emission phase shift φ can be directly measured by a phase fluorimeter and converted into the luminescence decay time τ according to Eq. 1:

$$\tau = \frac{\tan(\varphi)}{2 \cdot \pi \cdot f} \quad (1)$$

where f is the modulation frequency.

The response of oxygen indicators in solutions of organic solvents is described by the Stern-Volmer equation (Eq. 2), where τ is the luminescence lifetime, τ_0 is the luminescence lifetime in absence of oxygen, K_{SV} is the Stern-Volmer constant and pO₂ is the oxygen partial pressure.

$$\frac{\tau_0}{\tau} = 1 + K_{SV} \cdot pO_2 \quad (2)$$

However, the response of polymer-immobilized dyes is not linear in most cases. The so called “two-site-model” postulates

the existence of two domains in the polymer characterized by different oxygen permeabilities and thus different Stern-Volmer constants (Eq. 3) (Carraway et al. 1991). This equation excellently describes the behavior of the porphyrin indicators immobilized in polystyrene and other matrices.

$$\frac{\tau_0}{\tau} = \frac{1}{\frac{z}{1+K_{SV1} \cdot pO_2} + \frac{1-z}{1+K_{SV2} \cdot pO_2}} \quad (3)$$

where K_{SV1} and K_{SV2} are the Stern-Volmer constants for the two different domains and z is the distribution coefficient.

The pH sensing materials rely on a fluorescent indicator belonging to the aza-BODIPY group. These dyes feature large molar absorption coefficients, good quantum yields, and excellent photostability (Jokic et al. 2012; Strobl et al. 2015). Most importantly, they are excitable in the red part of the spectrum and emit in the near infrared region, thus being fully compatible with the optoelectronic unit (Fig. 2b). The indicator shows strong fluorescence when protonated which is completely quenched upon deprotonation. Although the dynamic range of optical pH sensors is typically limited to ± 1.5 pH units around the pK_a value of the indicator dye, this is not critical providing that an indicator adequate for the envisaged application is found. Therefore, the mono-hydroxyphenyl-substituted aza-BODIPY dye was chosen to cover the pH range between 7 and 8.5 required for marine applications.

The sensing materials employed in this work utilize a cross-linked copolymer of 99% acryloylmorpholine and 1% hydroxyethyl acrylamide as a proton-permeable hydrogel matrix. The indicator dye was covalently coupled to the matrix polymer, which is cross-linked with the commercially available polyisocyanate crosslinker Desmodur[®] N75 MPA/X from Covestro AG. The covalent coupling of the dye and crosslinking of the matrix improves the long-term stability of the sensing material by preventing the dye from leaching or migrating into the polymeric support (poly(ethylene terephthalate)). Whereas the material “pH 1” is covalently coupled to the matrix during the cross-linking process, in the second material (“pH 2”) the pH indicator is first coupled to the polymer which is then cross-linked in the following step. The detailed procedures for the preparation of the sensing materials are provided in the Supporting Information.

Since fluorescence is an ambiguous parameter, which is influenced by the intensity of the excitation light, sensitivity of the photodetector, concentration of the indicator, and thickness of the sensing film, a DLR scheme (Klimant et al. 2001) is utilized to enable reliable read-out. For this purpose, an additional layer containing calcium copper silicate (Egyptian blue) in form of a microcrystalline powder (Borisov et al. 2013) is added onto the opposite site of the transparent support. Egyptian blue is an inorganic phosphor which shows excitation and emission spectra matching the optical set-up (Fig. 2b) and is inert to pO₂, pH, and pCO₂. It features

a long luminescence decay time (107 μ s (Accorsi et al. 2009)) so that the overall phase shift measured by the phase fluorometer is proportional to the fluorescence amplitude of the indicator (A_{ind}) and thus the concentration of its protonated form:

$$\cot(\varphi_m) = \cot(\varphi_{ref}) + \frac{1}{\sin(\varphi_{ref})} \cdot \frac{A_{ind}}{A_{ref}} \quad (4)$$

where φ_m is the measured overall phase shift, and φ_{ref} and A_{ref} are the phase shift and the amplitude of the reference, respectively (both are constant for a given composition of the sensing material).

The pCO₂ sensing material has been presented elsewhere (Fritzsche et al. 2017). The detailed procedure for the preparation of the pCO₂ planar sensors is provided in the Supporting Information. It relies on a colorimetric aza-BODIPY indicator showing pCO₂-dependent absorption in the NIR part of the spectrum (Fig. 2c). The sensing material is of the so called “plastic type” (Mills et al. 1992; Mills and Monaf 1996). The indicator dye is immobilized in ethyl cellulose together with tetraoctylammonium hydroxide as a lipophilic base. This indicator layer is covered by a water and proton impermeable, but highly carbon dioxide-permeable Hyflon AD 60 layer. Hence the indicator dye is in its deprotonated form (dianionic form) at low pCO₂ and becomes protonated (monoanionic form) at high carbon dioxide partial pressures. An indicator with a high pK_a value (10.3 for the second deprotonation equilibrium of the dihydroxy aza-BODIPY dye; Schutting et al. 2015) was chosen to ensure sufficient sensitivity for measurements of atmospheric pCO₂ levels. Importantly, neither the monoanionic nor the dianionic forms of the dye are fluorescent, but the absorption maximum shifts from 745 nm to 805 nm upon the second deprotonation (Fig. 2c) (Schutting et al. 2015). In order to convert this analytical information into luminescence phase shift, two types of luminescent materials are added into the reference layer to make use of the inner-filter effect. The fluorescence emission of the first phosphor (dibutoxy aza-BODIPY, λ_{max} 733 nm) overlaps with the absorption of the monoanionic form of the indicator, whereas the emission of the inorganic phosphor (Egyptian blue, λ_{max} 908 nm; Schutting et al. 2015) shows excellent overlap with the absorption of the dianionic form. Overall phase shift depends on the ratio of both emissions and therefore is the highest at high pCO₂ (low intensity of fluorescence and high intensity of phosphorescence) and is the lowest at low pCO₂. Thus, this scheme enables quantification of pCO₂ via referenced phase shift measurement similar to DLR.

Temperature and salinity compensation

As expected, all three sensing materials show cross-sensitivity to temperature. Due to this fact, and because temperature itself is an important parameter in oceanographic measurements, a temperature sensor was incorporated into

the device. The response of the pH optodes is also influenced by ionic strength and therefore salinity, albeit to a much lesser extent. This cross-talk is marginal in ocean water but in other environments (brackish water) has to be compensated with help of external salinity data. Salinity data can be obtained via conventional conductivity measurement or using a recently reported sodium optode (Müller et al. 2017).

Characterization and calibration of the optodes

Characterization of the pH sensing materials was conducted by recording temperature and salinity calibrations in artificial seawater (Dickson et al. 2007) with a mixture of buffer substances (all obtained from Carl Roth GmbH & Co KG [www.carlroth.com]). Details about the buffer composition and measurement procedure can be found in the Supporting Information. The set pH values were measured with a glass pH electrode calibrated against spectrophotometric measurements (Easley and Byrne 2012) and pH values were calculated according to Liu et al. (2011).

The long-term stability test was performed in artificial seawater buffered with 50 mM TRIS. The pH changes were induced via addition of NaOH or HCl. The composition of the solution and the detailed procedures are provided in the Supporting Information.

The oxygen optodes were calibrated prior to deployments with air-saturated and oxygen-free water. Air-saturated water was obtained by repeated vigorous shaking of a water bottle. Five percentage aqueous solution of sodium sulfite with a catalytic amount of cobalt(II) chloride was used to ensure anoxic conditions.

Prior to deployments pH optodes were recalibrated with two calibration buffers based on TRIS and BIS-TRIS. This recalibration was conducted to determine the Top and Bottom coefficients of the calibration equation (see below), which are influenced by the indicator-to-reference ratio, and optical setup and may be different between individual sensor spots. The buffers were prepared for the in-field calibration of the pH-optodes based on a recipe for artificial seawater (Dickson et al. 2007). The recipes can be found in the supporting Information.

The pCO₂ optodes were calibrated prior to deployments at three different carbon dioxide levels. A 0.1 M phosphate buffer with a pH of 7.7 (NBS scale, 23°C) and a salinity of 9.4 was prepared and flushed with nitrogen for 2 h to remove dissolved carbon dioxide. Dissolved inorganic carbon (DIC) levels of 751 μM and 3415 μM were set by addition of an 890 mM sodium bicarbonate solution into this buffer. The corresponding carbon dioxide concentrations were calculated according to the constants determined by Roy et al. (1993). Thereby, the temperature dependence of the phosphate buffer was considered. The response of the optode was measured until a stable signal was reached (> 1.5 h). Additionally, a third calibration point (complete saturation of the optode with carbon dioxide) was recorded using soda water

(30 min). After the calibration, the sensor material was kept wet prior to deployment (Fritzsche et al. 2017).

Reference values

Discrete water samples were taken manually from Niskin bottles at different depths to validate the obtained data for oxygen, pH, and carbon dioxide. Two samples (250 mL) were taken at each depth and poisoned with saturated mercury chloride (100 μL) right after sampling. Total alkalinity (TA), DIC, and pH were measured for each sample. DIC was measured using a SOMMA system (Single Operator Multi-Parameter Metabolic Analyzer) at 15°C (Dickson et al. 2007). TA was obtained by using an open-cell titration at 20°C (Dickson et al. 2007). The indicator dye *m*-cresol purple was used to measure the pH spectrophotometrically at 25°C (Mosley et al. 2004). The CO2SYS program by Lewis and Wallace 1998 (Pierrot et al. 2011) was used to calculate the carbon dioxide concentrations (from DIC and pH values) with the constants from Roy et al. (1993) and the pH at in situ conditions in total scale.

Assessment

Temperature and salinity cross-talk of the pH optodes

The response of the pH sensing material is influenced by temperature and salinity. Therefore, prior to measurements, the salinity and temperature cross-talk of the sensor was investigated. For the tests in the Baltic Sea, the calibration curves for temperatures between 4°C and 15°C and salinities of 3 PSU, 6.5 PSU, and 10 PSU were recorded for the material “pH-1.” The sensor material “pH-2” was characterized between 0°C and 25°C at salinity 35. The calibration curves (Fig. 3a) were fitted with a Boltzmann sigmoid function:

$$\cot \varphi = \text{Bottom} + \frac{\text{Top} - \text{Bottom}}{1 + 10^{\frac{\text{pH} - \text{V50}}{\text{slope}}}} \quad (5)$$

where (dPhi) is the phase angle, Bottom is the lower limit of the calibration curve, Top is the upper limit of the calibration curve, pH is the pH value and V50 is the point of inflection, and slope describes the slope at the point of inflection. The same data points were fitted with additional temperature coefficients for the V50, Top, and Bottom coefficients:

$$\cot \varphi = \text{Bottom} + B_t \cdot (T - 20) + \frac{\text{Top} + T_t \cdot (T - 20) - (\text{Bottom} + B_t \cdot (T - 20))}{1 + 10^{\frac{\text{pH} - (\text{V50} + \text{V50}_t \cdot (T - 20))}{\text{slope}}}} \quad (6)$$

where B_t , T_t , and V50_t are the additional linear temperature coefficients for the Bottom, Top, and V50 coefficients, respectively, and T is the temperature in °C. Equation 6 was used for all measurements without salinity compensation. The recorded calibration points were fitted with this equation to obtain V50, slope, and the temperature coefficients. Individual calibrations of the sensor spots were conducted

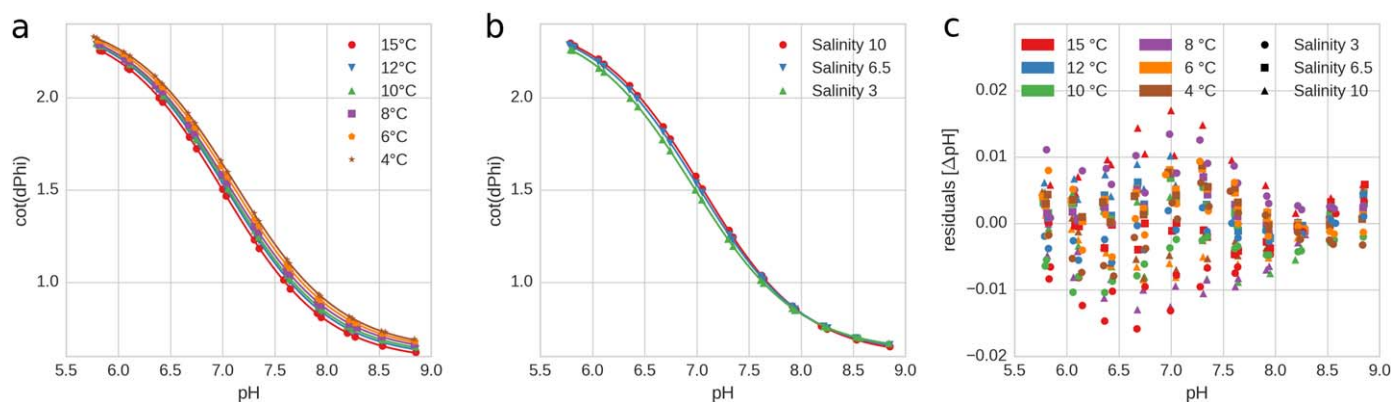


Fig. 3. Temperature and salinity calibration of the pH sensing material “pH-1.” Fig. 6a Calibration curves at salinity 10 for temperatures between 4°C and 15°C, fitted with a Boltzmann sigmoid; **(b)** Calibration at salinities 3, 6.5, and 10 at constant temperature of 10°C; **(c)** Residuals of the fit-function with coefficients for temperature and salinity; the same calibration curves fitted with temperature coefficients for V50, Top, and Bottom.

by fitting the Top and Bottom coefficients after measuring buffers in artificial seawater.

Due to an expected salinity sensitivity at the low salinities of the Baltic Sea, the ionic strength dependency of the sensing material pH-1 was characterized between 3 PSU and 10 PSU (Fig. 3b). For every tested salinity, temperature calibrations at 4°C, 6°C, 8°C, 10°C, 12°C, and 15°C were recorded (18 calibration curves total, Fig. 3). A small cross-talk is evident for about threefold salinity increase. To compensate for this cross-talk, additional coefficients for V50 and Bottom were introduced (Eq. 7) and simultaneous fitting of all recorded data points (4–15°C; 3 PSU, 6.5 PSU, 10 PSU) was performed.

$$\text{cot(dPhi)} = \text{Bottom} + B_t \cdot (T-20) + B_s \cdot (S-35) + \frac{\text{Top} + T_t \cdot (T-20) - (\text{Bottom} + B_t \cdot (T-20) + B_s \cdot (S-35))}{1 + 10^{\frac{\text{pH} - (V50 + V50_t \cdot (T-20) + V50_s \cdot (S-35))}{\text{slope}}}} \quad (7)$$

where B_s and $V50_s$ are linear salinity coefficients for the Bottom and V50 parameters and S is the salinity in PSU. This calibration curve has three independent parameters and can therefore not be plotted. In contrast to the conditions in the Baltic Sea, the salinity of ocean water is nearly constant (~ 35 PSU) and the minor variations do not affect the response of the sensor, and therefore, no compensation for these fluctuations is required. The residuals of the calibration of sensing material “pH-2” were equal to that of “pH-1” presented in Fig. 3.

Stability test of the pH and oxygen sensor materials

Figure 4 depicts a simulated long-term deployment (> 40 d) in artificial seawater (volume 50 L) conducted for the pH and oxygen sensing materials. The experimental details can be found in the Supporting Information. The long-term stability of the carbon dioxide sensor was already assessed elsewhere (Fritzsche et al. 2017) in a similar experiment over 35 d. Thereby, no indication of sensor poisoning or drift was

found. The oxygen sensors were tested over 48 d and the pH sensors over 42 d at approximately 24°C. The sensors recorded one measurement point every 30 s, which corresponds to approximately 120,000 and 140,000 measurement points for the pH and oxygen sensor materials, respectively. The pH value was changed by addition of 250 mL 0.72 M hydrochloric acid on day 8, 21, 22, 23 and the addition of 40 mL 40% NaOH on day 10 and 10 mL on the days 41, 42, 43. The spectrophotometric pH measurements were always conducted at 23°C and converted to in situ conditions with a TRIS temperature coefficient of $-0.0313/\text{K}$ at salinity 35 (DelValls and Dickson 1998). The measured pO_2 values were converted with the oxygen solubility constants determined by Garcia and Gordon (1992).

During most deployments, lower temperatures and longer sampling intervals and hence lower stress on the materials can be expected. At these rather high temperatures, we observed a drift of the sensor signal (approximately $0.003 \text{ pH units d}^{-1}$) indicating that a drift correction was necessary for long-term measurements. The drift of the sensor materials is predictable and characterized by a decrease in maximum fluorescence intensity, which results in a decrease of the Top coefficient and hence a reduction in sensor dynamics (Top–Bottom). Therefore, it was possible to determine the drift constant and correct the sensor readings (Supporting Information). However, the drift constant is temperature dependent and much lower at lower temperatures. At 10°C, the drift constant was determined as 0 and therefore no drift correction was applied to the measurements during the field trips. It is evident that after the performed correction, the pH sensors show stable performance over 1.5 months of continuous operation, and the calculated pH values correlate well to the values obtained in the reference spectrophotometric measurement (Fig. 4). The readings provided by the five pH sensors match very well (correlation coefficients > 0.9987). The precision of the pH sensor was excellent with average

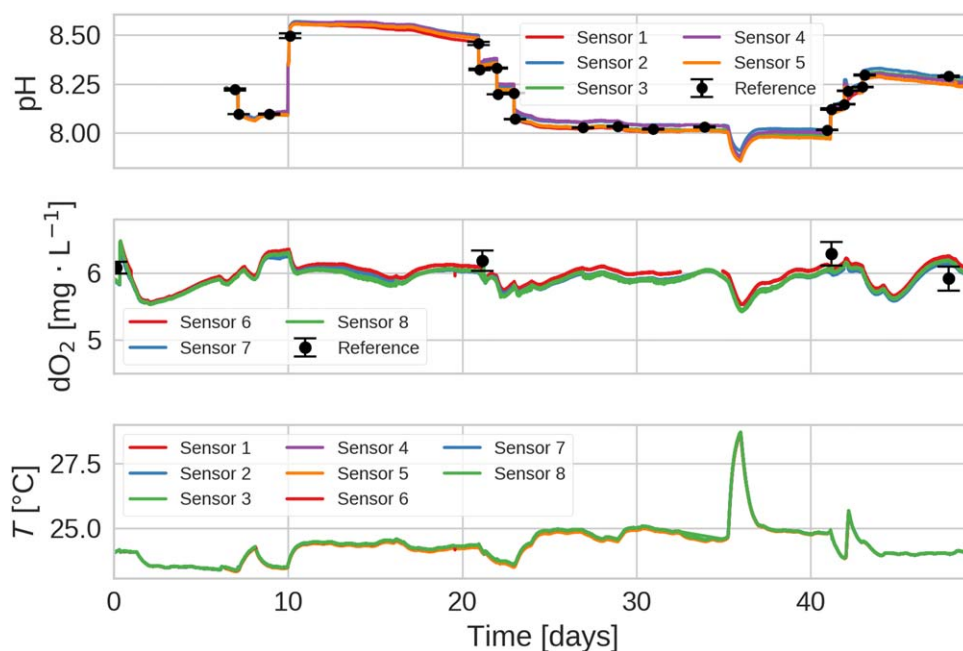


Fig. 4. Stability measurement of the pH and pO₂ sensor materials. Sensors 1–5 are pH sensors based on the material pH-2; sensors 6–8 are oxygen sensors. Changes in pH were induced by addition of either a 0.72 M hydrochloric acid or a 40% sodium hydroxide solution. The sharp increase of DO on day 1 is due to bubbling of pressurized air through the buffer for 1 h. Reference values were obtained by sampling and spectrophotometric pH measurements and Winkler titration for pH and oxygen, respectively. The temperature spike on day 35 was induced by the waste heat of a nearby device. The missing data of sensor 6 was caused by an unexpected restart of a computer used for data logging.

standard deviations of 0.0023 and 0.0019 pH units for pH \sim 8.02, and \sim 8.55, respectively. The standard deviations were determined over periods with nearly constant pH and temperature (day 11–13 for pH \sim 8.55 and day 25–32 for pH \sim 8.02). The pH drift of the buffer due to uptake of carbon dioxide was compensated linearly for these calculations and the minor fluctuations of pH of the TRIS-buffer due to temperature changes were compensated according to literature (DeIValis and Dickson 1998). The accuracy of the sensors can be estimated by their average absolute deviation from the reference values which was 0.020 pH units. The oxygen sensor materials required no drift compensation and fit well to the recorded reference points throughout the experiment with an average absolute deviation of 0.25 mg L⁻¹. Furthermore, they showed good correlation between each other with correlation coefficients above 0.974.

This stability test demonstrates that the sensing materials can be used for deployments of at least 1.5 months and more than 100,000 single measurement points can be recorded. However, in real world applications long deployments may require protection against biofouling. This issue was not the aim of the current work since only short term deployments were envisaged, but it has to be addressed in future to broaden the application range of the sensors.

Application of the optode system for profiling in the Baltic Sea

An application of the optode system was demonstrated during a research cruise in the Baltic Sea in October 2015. Overall 12 devices were deployed. The number of deployed oxygen, pH, and carbon dioxide optodes was varied throughout the field trip.

During the cruise, overall 12 profiles with multiple optodes and analytes to a maximum depth of 230 m were recorded. Examples of the measured depths profiles are displayed in Fig. 5. Oxygen, pH, and carbon dioxide optodes were deployed simultaneously for this measurement. Since the carbon dioxide dynamics is large and the response of the carbon dioxide sensors is slow ($t_{90} > 1$ h) at temperatures below 15°C, stops were made during the downcast to allow for complete equilibration of the carbon dioxide sensors. During these stops, samples for reference measurements were taken. Unfortunately, no reference values for dissolved oxygen (DO) could be obtained due to a failure of the oxygen sensor of the CTD-probe. As can be seen, concentration of DO strongly decreases below 50 m. Although the concentration approaches 0 below the halocline, at around 70 m water depth, a significant increase to about 50 μ M is visible between 150 m and 220 m. This effect can be explained by a strong inflow of oxygen rich saltwater from the North Sea in December 2014 (Gräwe et al. 2015; Mohrholz et al. 2015).

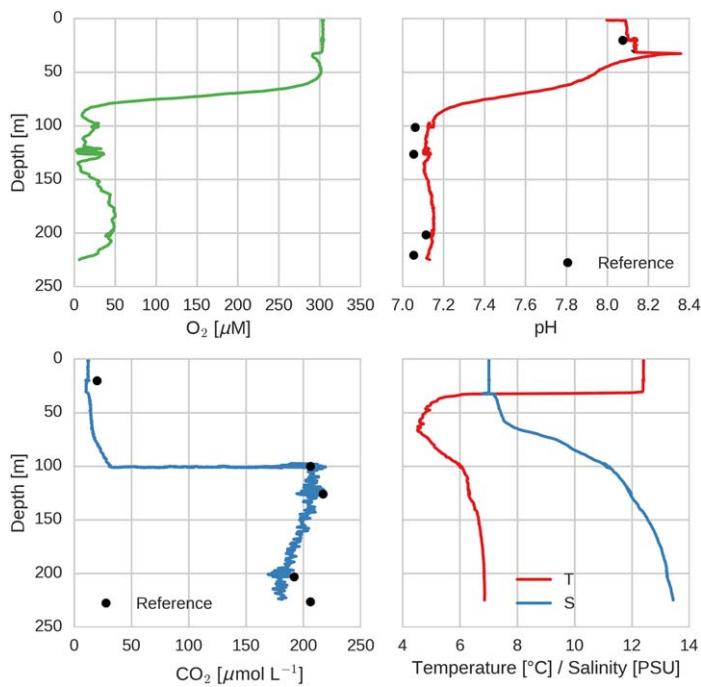


Fig. 5. Profiles recorded at the Gotland deep monitoring station BY15 [Sta. 5 in (a), GPS: 57.32041, 20.05197], five stops at 20 m (1 h 30 min), 100 m (1 h), 120 m (1 h), 200 m (1 h 50 min), and 230 m (45 min) water depth to allow equilibration of the carbon dioxide sensor. The CTD was lowered with a speed of 0.15 m s⁻¹. Reference values were obtained by DIC and spectrophotometric pH measurements from samples. The pH spike at ~ 30 m is an artifact caused by the different response times of the pH sensor material and the temperature sensor used for correction of the temperature cross-talk.

The pH profile mirrors that of oxygen demonstrating a strong pH decrease (1 pH unit) at the depth below 70 m. This is expected because microbial respiration consumes oxygen and produces carbon dioxide which results in a decrease of pH. Again, a slight increase of pH of around 0.05 pH units is clearly visible between 150 m and 220 m. The profiles obtained by the pH optode are in good agreement with the reference values with an average absolute difference between the optode and the spectrophotometric reference measurements of 0.033 pH units over all 10 recorded profiles. On average, the optode recorded 0.013 pH units higher values than the spectrophotometric reference. This deviation is probably due to calibration errors in the low salinity environment of the Baltic Sea. The obtained profile for carbon dioxide shows a trend consistent to the other two optodes. However, between 70 m and 100 m, the profile is distorted due to the long response time of the carbon dioxide optode (*t*₉₀ approximately 1 h) and very large changes in the carbon dioxide concentration (15–200 μM). Nevertheless, after equilibration of the sensor at the depth of 100 m (1 h stop), the reading obtained by the optode matches very well with the reference data. Again, the concentration of carbon dioxide was nearly constant

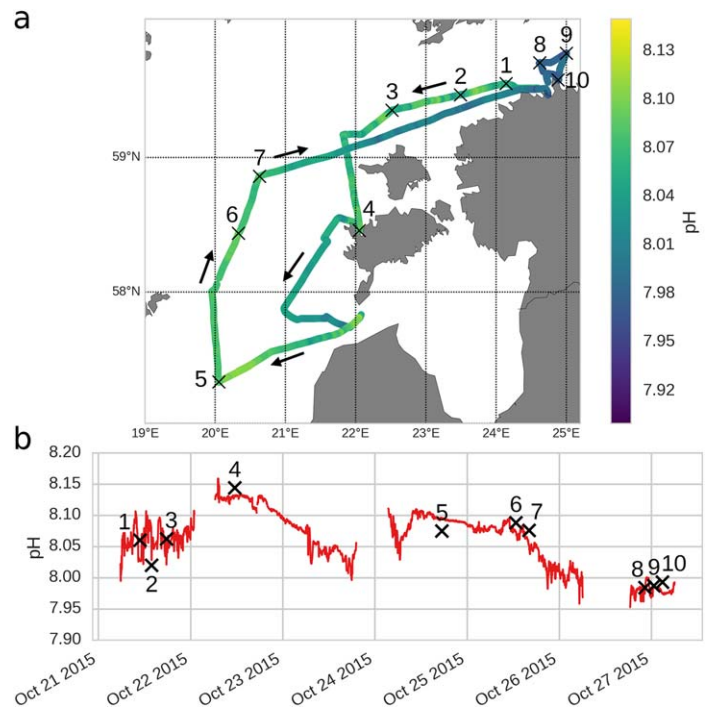


Fig. 6. Continuous measurement of the surface pH during the cruise in the Baltic Sea. pH values are color coded in the upper part of the figure (a) and plotted against time in the lower part of the figure (b). Reference values (1–10) were obtained from samples of the mixed upper water layer during profiling. During stops in harbors, the measurements were interrupted resulting in the breaks in the time series. The sensor was calibrated at the start of the measurement and recalibrated on the 24th of October.

below 70 m. About 10-fold increase of the carbon dioxide concentration between the surface water and the depth of 100 m correlates very well with the pH decrease of about 1 pH unit. It should be noted that this profile was presented by Fritzsche et al. (2017) without the corresponding pH and O₂ data. Compared to the previous presentation of the carbon dioxide data, additional corrections have been made: (1) temperature influence on the calibration buffers was accounted for and (2) the pH of the buffers was converted to total scale to be compatible with the coefficients reported by Roy et al. (1993).

Overall similar trends are visible from all three sensing materials. The average pH deviation between the optode and the reference measurements for the cast depicted in Fig. 5 was 0.051 pH units and the average deviation in carbon dioxide concentration was 12 μM. These measurements demonstrate that this novel optode system is capable of a simultaneous measurement of all parameters required to fully characterize the carbonate system.

Continuous surface water pH measurements

Throughout the same field survey in the Baltic Sea, a FerryBox system (equipped with a seawater pump and a pH optode) was used for continuous pH measurements of the surface water for 7 d.

Spectrophotometric reference points for these measurements were obtained from samples taken from the mixed water column during the profiles. The breaks in the measurement on 21st, 23rd/24th, and 26th of October are due to shutdowns of the system during stops in harbors. During the stop on 24th October, the pH sensor was recalibrated. As can be seen in Fig. 6, the data for the surface pH obtained with the optode are in good agreement with the reference points. The average absolute deviation from the reference measurements was 0.019 pH units.

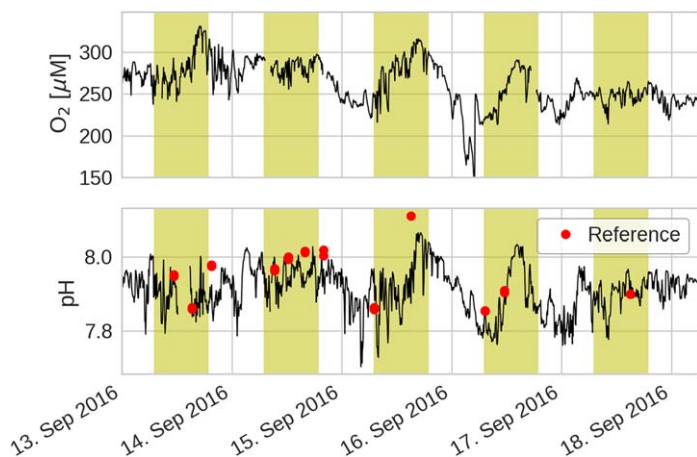


Fig. 7. Simultaneous measurement of pH and O₂ with two optodes in the harbor of Kiel in 2–4 m water depth (GPS: 54.330168, 10.149846). The pH reference values were recorded spectrophotometrically on discrete water samples. The yellow areas indicate the time between sunrise and sunset.

Simultaneous monitoring of oxygen and pH in Kiel harbor

During a field-survey in Kiel, Germany, oxygen and pH optodes were deployed in combination over the course of 5 d. Throughout the deployment, pH reference values were obtained by spectrophotometric measurements of discrete water samples.

The system dynamics measured by the oxygen and pH optodes shows good correlation (Fig. 7). High oxygen concentration corresponds to high pH values and a Pearson correlation coefficient of 0.54 is obtained between the two variables. This is likely due to photosynthetic activity of algae in the water masses. High photosynthetic activity results in an increase in oxygen concentration and, due to the consumption of carbon dioxide, in high pH values. This correlation is visible in the daily fluctuations. Smaller fluctuations are likely to be due to the movement of water masses with the waves in the harbor (Geißler et al. 2017). Since both optodes were not positioned at the same depth, the smaller changes in concentration of DO and pH are not always identical. The average deviation from the reference values was 0.043 pH units without the outlier on 15th September. The pH optode was calibrated before and after the deployment, whereby the post calibration, which was used for the evaluation of the data, resulted in pH values which are on average 0.035 pH units higher.

This somewhat larger difference compared to the open sea measurements presented above can presumably be attributed to the higher small-scale heterogeneity of coastal seawater carbonate chemistry. The outlier on 15th September is probably due to incomplete mixing of the water layers during the sharp increase in pH. During the field survey in Kiel, several other sensors developed in the SenseOcean project

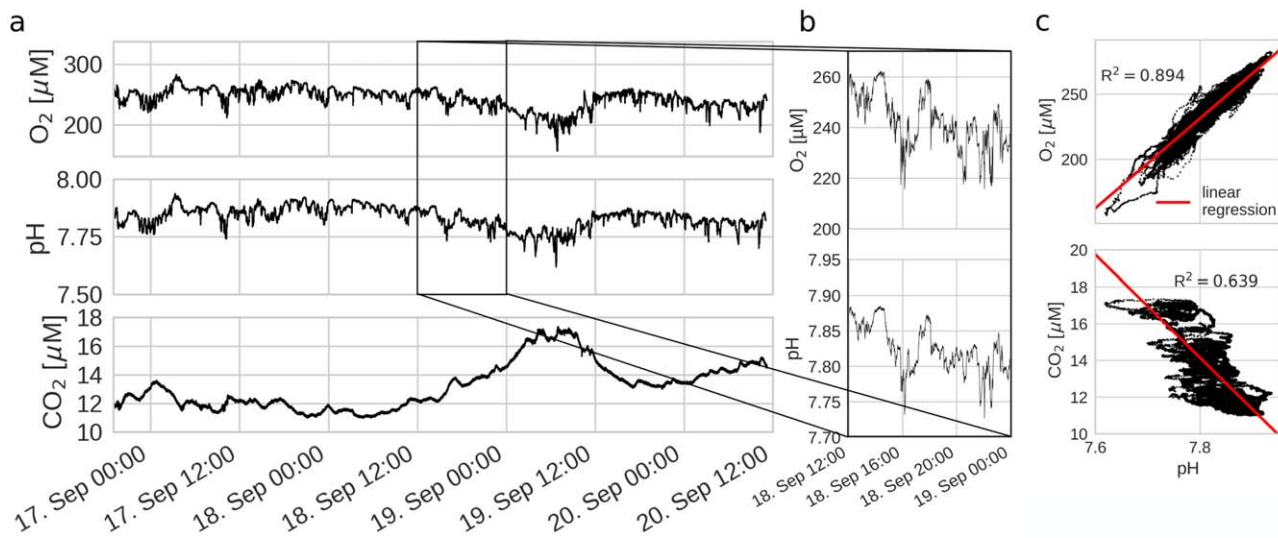


Fig. 8. (a) Simultaneous measurement of pH, DO, and carbon dioxide with an array of three optodes in the harbor of Kiel (GPS: 54.330168, 10.149846) in approximately 2 m water depth. (b) The inset shows the fast fluctuations resolved by the pH and oxygen optodes. (c) Correlation plots between pH and DO/carbon dioxide.

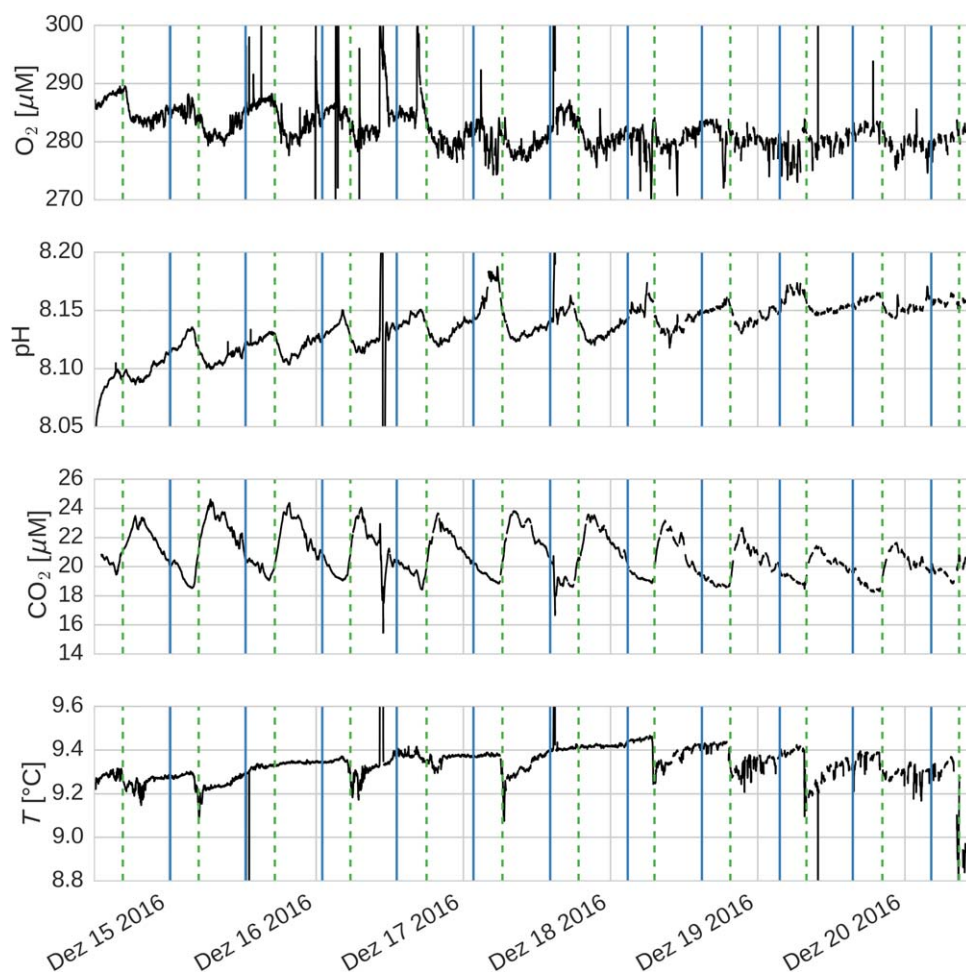


Fig. 9. Simultaneous measurement of pH, DO, and carbon dioxide with the optode system over 6 d on a pier in Southampton (~ 3 m water depth). The vertical solid blue lines and the dashed green lines indicate times of high and low tide, respectively. The artifacts on 16th December were caused by a short removal of the sensors. The displayed temperature data was recorded by the temperature sensor integrated into the oxygen optode.

were deployed alongside a pontoon and the water samples were collected approximately 10 m from the optodes.

Figure 8 shows the results of a similar experiment in Kiel harbor in which all the three optodes (pH, pO_2 , and pCO_2) were positioned in exactly the same depth in the close proximity to each other (< 50 cm). It is evident that all the optodes show good correlation over the period of 3 d. Pearson correlation coefficient of 0.945 and -0.8 are obtained between pH and DO, and pH and dissolved carbon dioxide, respectively. Moreover, the pO_2 and the pH optodes, which are much faster than the pCO_2 optode, resolve exceptionally well the minor changes of parameters. In fact, every fluctuation in the concentration of DO is also registered by the pH optode. Even fluctuations faster than 1 min and smaller than 0.01 pH units and $3 \mu\text{M}$ DO are clearly visible. This demonstrates the advantages of the new optode system which is suitable for continuous monitoring of the important parameters with time resolution better than 5 min and is capable of resolving even minor fluctuations of these parameters ($<$

0.005 pH units). Some of the finer scale dynamic changes were still registered by the pCO_2 optode but most of the peaks were “smoothed” due to longer response time of more than 1 h. The long-response time also complicates the calibration of the pCO_2 optode and increases the error since the sensor may not reach the full equilibration during the calibration. Nevertheless, although the pCO_2 optode is currently unable to compete with the pO_2 and pH optodes in terms of response time, we are optimistic that significant improvements to the sensor chemistry can be made in future.

Simultaneous monitoring of pH, DO, and carbon dioxide in Southampton harbor

During the field-survey to Southampton, England, optodes with O_2 , pH, and pCO_2 sensing materials were used for continuous measurement within 1 week (Fig. 9). The oxygen sensor shows periodic fluctuations of the oxygen concentration ($\sim 5 \mu\text{M}$). Interestingly, a slow decrease of the oxygen saturation ($287\text{--}280 \mu\text{M}$) is visible during the field work. The pH sensors show very similar short term results. Periodic fluctuations

of approximately 0.04 pH-units are visible and synchronized to the DO fluctuations. Overall, a slight increase of pH (ca. 0.05 pH units) is visible during the field trip. The pCO₂ sensor displays again very similar fluctuations and a slight decrease of the carbon dioxide concentration (ca. 1 μM) toward the end of the experiment. The temperature sensor displays values between 9.5°C and 8.8°C and most of the temperature changes are very slow. As can be seen in Fig. 9, the data acquired for the three parameters correlate well. Pearson correlation coefficient of 0.822 and -0.901 are obtained between pH and DO, and pH and dissolved carbon dioxide on the 15th of December, respectively. This day was chosen because no artifacts influenced the measurements. In fact, every decrease in oxygen concentration is mirrored by a decrease in pH and an increase in pCO₂. Even very small fluctuations are often visible on all three traces, whereby high pO₂ and pH and low pCO₂ indicate water masses with weak photosynthetic activity and vice versa.

Besides the short term fluctuations, the 5-d profiles recorded by the sensors are very interesting. All three sensors display a reduction of the amplitude of the periodic fluctuations over the course of the measurement. Furthermore, there is a weak decrease in DO (~ 5 μM) and dissolved carbon dioxide (~ 2 μM) visible with a slight increase in pH (~ 0.05 pH units). While this might be due to sensor drift, it is noted that all three sensing materials display a similar trend. Comparison of the acquired data with the tidal range over the course of the measurement (4.12 m on 15th December and 2.82 m on 20th December) suggests that the reductions in amplitude are probably due to a reduction in water exchange. This reduced exchange of Southampton water could as well influence the mean values of pO₂, pH, and pCO₂. It is also evident, that the changes in the parameters within 1-d cycle correlate well with the periods of low and high tide. As can be seen in Fig. 9, shortly before every low tide maxima of DO and pH and minima of carbon dioxide were visible.

Another demonstration of the sensor system was conducted in a seagrass field in Aggersund, Denmark during a 4-d deployment (Supporting Information Fig. S1). Pronounced day/night fluctuations of the local oxygen saturation were observed. The concentration of DO reached values as high as 500 μM which corresponds to 250% of air saturation during the day whereas the conditions are nearly anoxic at night. More detail on this experiment can be found in the Supporting Information.

Conclusions

In conclusion, a small and cost-effective optode system for measurement of three important oceanographic parameters is presented. The very energy efficient read-out device (1.4 million measurement points when fully charged) enables deployments over 1 yr potentially without any service and the small and light design simplifies the integration of the optode in many already existing set-ups. Although the long-term

stability of the sensing materials for such long-deployment periods has not been accessed yet, the laboratory trials (comparably high temperature of 24°C, over 100,000 measurement points) demonstrated stable performance of the sensors for over 1 month of continuous operation. These results suggest that the sensing materials can operate reliably over significantly longer timescale, but other issues such as biofouling are likely to be more critical for long-term deployment and should be addressed in future.

Importantly, the flexible design of the optode system enables fast exchange of the analyte of interest or the dynamic range (e.g., normal range or trace oxygen sensor) via a screwable sensor cap. This is achieved by using a shared optoelectronic unit and selecting a set of “sensing chemistries” with optical properties matching the opto-electronic components of the read-out device. This approach greatly facilitates adaptation of the sensor setup on-site. The sensor system has been applied successfully in several field trips and the results show good correlation between all measured parameters and clearly demonstrate the advantages of the new optode system for continuous monitoring of pH, DO, and carbon dioxide. Whereas the pH and oxygen optode deliver excellent time resolution with response times (t_{90}) below 1 min (without optical isolation) and resolve minor fluctuations of these parameters, the pCO₂ optode “smoothes” the dynamics due to slower response time. While the accuracy and precision of the pH and carbon dioxide optodes is not yet good enough for ocean acidification studies without additional reference measurements, the optode system is likely to be very useful especially for measurements requiring high spatial or temporal resolution. It can greatly simplify and reduce the costs of alternating measurements of pH, O₂, and carbon dioxide as only one type of device with estimated hardware costs of around 1000 Euro is necessary. Therefore, the sensor system already now offers vast possibilities for oceanographic applications and can be extended in future for sensing of other parameters (e.g., ions) providing that the new “sensing chemistries” matching the optoelectronic set-up of the read-out device are developed.

References

- Accorsi, G., G. Verri, M. Bolognesi, N. Armaroli, C. Clementi, C. Miliani, and A. Romani. 2009. The exceptional near-infrared luminescence properties of cuprorivaite (Egyptian blue). *Chem. Commun.* 3392–3394. doi:10.1039/b902563d
- Amao, Y., and N. Nakamura. 2004. Optical CO₂ sensor with the combination of colorimetric change of α -naphtholphthalein and internal reference fluorescent porphyrin dye. *Sens. Actuators B Chem.* **100**: 347–351. doi:10.1016/j.snb.2004.02.003
- Atamanchuk, D., A. Tengberg, P. J. Thomas, J. Hovdenes, A. Apostolidis, C. Huber, and P. O. J. Hall. 2014.

- Performance of a lifetime-based optode for measuring partial pressure of carbon dioxide in natural waters. *Limnol. Oceanogr.: Methods* **12**: 63–73. doi:10.4319/lom.2014.12.63
- Borisov, S. M., C. Würth, U. Resch-Genger, and I. Klimant. 2013. New life of ancient pigments: Application in high-performance optical sensing materials. *Anal. Chem.* **85**: 9371–9377. doi:10.1021/ac402275g
- Bresnahan, Jr., P. J., T. R. Martz, Y. Takeshita, K. S. Johnson, and M. LaShomb. 2014. Best practices for autonomous measurement of seawater pH with the Honeywell Durafet. *Methods Oceanogr.* **9**: 44–60. doi:10.1016/j.mio.2014.08.003
- Byrne, R. H., and J. A. Breland. 1989. High precision multi-wavelength pH determinations in seawater using cresol red. *Deep-Sea Res. Part A Oceanogr. Res. Pap.* **36**: 803–810. doi:10.1016/0198-0149(89)90152-0
- Caldeira, K., and M. E. Wickett. 2003. Oceanography: Anthropogenic carbon and ocean pH. *Nature* **425**: 365–365. doi:10.1038/425365a
- Carraway, E. R., J. N. Demas, B. A. DeGraff, and J. R. Bacon. 1991. Photophysics and photochemistry of oxygen sensors based on luminescent transition-metal complexes. *Anal. Chem.* **63**: 337–342. doi:10.1021/ac00004a007
- Clarke, J. S., E. P. Achterberg, V. M. C. Rérolle, S. Abi Kaed Bey, C. F. A. Floquet, and M. C. Mowlem. 2015. Characterisation and deployment of an immobilised pH sensor spot towards surface ocean pH measurements. *Anal. Chim. Acta* **897**: 69–80. doi:10.1016/j.aca.2015.09.026
- Clarke, J. S., E. P. Achterberg, D. P. Connelly, U. Schuster, and M. Mowlem. 2017. Developments in marine pCO₂ measurement technology; towards sustained in situ observations. *TrAC Trends Anal. Chem.* **88**: 53–61. doi:10.1016/j.trac.2016.12.008
- Clayton, T. D., and R. H. Byrne. 1993. Spectrophotometric seawater pH measurements: Total hydrogen ion concentration scale calibration of m-cresol purple and at-sea results. *Deep-Sea Res. Part I Oceanogr. Res. Pap.* **40**: 2115–2129. doi:10.1016/0967-0637(93)90048-8
- Covington, A. K., and M. Whitfield. 2009. Recommendations for the determination of pH in sea water and estuarine waters. *Pure Appl. Chem.* **60**: 865–870. doi:10.1351/pac198860060865
- DeGrandpre, M. D., T. R. Hammar, S. P. Smith, and F. L. Sayles. 1995. In situ measurements of seawater pCO₂. *Limnol. Oceanogr.* **40**: 969–975. doi:10.4319/lo.1995.40.5.0969
- DeGrandpre, M. D., M. M. Baehr, and T. R. Hammar. 1999. Calibration-free optical chemical sensors. *Anal. Chem.* **71**: 1152–1159. doi:10.1021/ac9805955
- DelValls, T. A., and A. G. Dickson. 1998. The pH of buffers based on 2-amino-2-hydroxymethyl-1,3-propanediol ('tris') in synthetic sea water. *Deep-Sea Res. Part I Oceanogr. Res. Pap.* **45**: 1541–1554. doi:10.1016/S0967-0637(98)00019-3
- Dickson, A. G. 1984. pH scales and proton-transfer reactions in saline media such as sea water. *Geochim. Cosmochim. Acta* **48**: 2299–2308. doi:10.1016/0016-7037(84)90225-4
- Dickson, A. G. 1993. The measurement of sea water pH. *Mar. Chem.* **44**: 131–142. doi:10.1016/0304-4203(93)90198-W
- Dickson, A. G., C. L. Sabine, J. R. Christian, C. P. Barger, and North Pacific Marine Science Organization [eds.]. 2007. Guide to best practices for ocean CO₂ measurements. North Pacific Marine Science Organization.
- Doney, S. C., V. J. Fabry, R. A. Feely, and J. A. Kleypas. 2009. Ocean acidification: The other CO₂ problem. *Annu. Rev. Mar. Sci.* **1**: 169–192. doi:10.1146/annurev.marine.010908.163834
- Easley, R. A., and R. H. Byrne. 2012. Spectrophotometric calibration of pH electrodes in seawater using purified m-cresol purple. *Environ. Sci. Technol.* **46**: 5018–5024. doi:10.1021/es300491s
- Fiedler, B., P. Fietzek, N. Vieira, P. Silva, H. C. Bittig, and A. Körtzinger. 2013. In situ CO₂ and O₂ measurements on a profiling float. *J. Atmos. Ocean. Technol.* **30**: 112–126. doi:10.1175/JTECH-D-12-00043.1
- Fietzek, P., B. Fiedler, T. Steinhoff, and A. Körtzinger. 2014. In situ quality assessment of a novel underwater pCO₂ sensor based on membrane equilibration and NDIR spectrometry. *J. Atmos. Ocean. Technol.* **31**: 181–196. doi:10.1175/JTECH-D-13-00083.1
- Friederich, G. E., P. G. Brewer, R. Herlien, and F. P. Chavez. 1995. Measurement of sea surface partial pressure of CO₂ from a moored buoy. *Deep-Sea Res. Part I Oceanogr. Res. Pap.* **42**: 1175–1186. doi:10.1016/0967-0637(95)00044-7
- Fritzche, E., P. Gruber, S. Schutting, J. P. Fischer, M. Strobl, J. D. Müller, S. M. Borisov, and I. Klimant. 2017. Highly sensitive poisoning-resistant optical carbon dioxide sensors for environmental monitoring. *Anal. Methods* **9**: 55–65. doi:10.1039/C6AY02949C
- Garcia, H. E., and L. I. Gordon. 1992. Oxygen solubility in seawater: Better fitting equations. *Limnol. Oceanogr.* **37**: 1307–1312. doi:10.4319/lo.1992.37.6.1307
- Geißler, F., and others. 2017. Evaluation of a ferrozine based autonomous in situ lab-on-chip analyzer for dissolved iron species in coastal waters. *Front. Mar. Sci.* **4**: 00322. doi:10.3389/fmars.2017.00322
- Gräwe, U., M. Naumann, V. Mohrholz, and H. Burchard. 2015. Anatomizing one of the largest saltwater inflows into the Baltic Sea in December 2014. *J. Geophys. Res. Oceans* **120**: 7676–7697. doi:10.1002/2015JC011269
- Hunt, C. W., L. Snyder, J. E. Salisbury, D. Vandemark, and W. H. McDowell. 2017. SIPCO₂: A simple, inexpensive surface water pCO₂ sensor. *Limnol. Oceanogr.: Methods* **15**: 291–301. doi:10.1002/lom3.10157
- Jiang, Z.-P., and others. 2014. Application and assessment of a membrane-based pCO₂ sensor under field and laboratory conditions. *Limnol. Oceanogr.: Methods* **12**: 264–280. doi:10.4319/lom.2014.12.264

- Jimenez-Jorquera, C., J. Orozco, and A. Baldi. 2009. ISFET based microsensors for environmental monitoring. *Sensors* **10**: 61–83. doi:10.3390/s100100061
- Johnson, K. S., H. W. Jannasch, L. J. Coletti, V. A. Elrod, T. R. Martz, Y. Takeshita, R. J. Carlson, and J. G. Connery. 2016. Deep-Sea DuraFET: A pressure tolerant pH sensor designed for global sensor networks. *Anal. Chem.* **88**: 3249–3256. doi:10.1021/acs.analchem.5b04653
- Jokic, T., S. M. Borisov, R. Saf, D. A. Nielsen, M. Köhl, and I. Klimant. 2012. Highly photostable near-infrared fluorescent pH indicators and sensors based on BF₂-chelated tetraarylazadipyromethene dyes. *Anal. Chem.* **84**: 6723–6730. doi:10.1021/ac3011796
- Klimant, I., C. Huber, G. Liebsch, G. Neurauder, A. Stangelmayer, and O. S. Wolfbeis. 2001. Dual lifetime referencing (DLR) — a new scheme for converting fluorescence intensity into a frequency-domain or time-domain information, p. 257–274. In P. B. Valeur and D. J.-C. Brochon [eds.], *New trends in fluorescence spectroscopy*. Springer.
- Larsen, M., P. Lehner, S. M. Borisov, I. Klimant, J. P. Fischer, F. J. Stewart, D. E. Canfield, and R. N. Glud. 2016. In situ quantification of ultra-low O₂ concentrations in oxygen minimum zones: Application of novel optodes. *Limnol. Oceanogr.: Methods* **14**: 784–800. doi:10.1002/lom3.10126
- Le Bris, N., and D. Birot. 1997. Automated pH-ISFET measurements under hydrostatic pressure for marine monitoring application. *Anal. Chim. Acta* **356**: 205–215. doi:10.1016/S0003-2670(97)00533-3
- Lefèvre, N., J. P. Ciabrini, G. Michard, B. Briant, M. DuChaffaut, and L. Merlivat. 1993. A new optical sensor for pCO₂ measurements in seawater. *Mar. Chem.* **42**: 189–198. doi:10.1016/0304-4203(93)90011-C
- Lehner, P., and others. 2015. LUMOS - A sensitive and reliable optode system for measuring dissolved oxygen in the nanomolar range. *PLoS One* **10**: e0128125. doi:10.1371/journal.pone.0128125
- Liu, X., Z. A. Wang, R. H. Byrne, E. A. Kaltenbacher, and R. E. Bernstein. 2006. Spectrophotometric measurements of pH in-situ: Laboratory and field evaluations of instrumental performance. *Environ. Sci. Technol.* **40**: 5036–5044. doi:10.1021/es0601843
- Liu, X., M. C. Patsavas, and R. H. Byrne. 2011. Purification and characterization of meta-cresol purple for spectrophotometric seawater pH measurements. *Environ. Sci. Technol.* **45**: 4862–4868. doi:10.1021/es200665d
- Lu, Z., M. Dai, K. Xu, J. Chen, and Y. Liao. 2008. A high precision, fast response, and low power consumption in situ optical fiber chemical pCO₂ sensor. *Talanta* **76**: 353–359. doi:10.1016/j.talanta.2008.03.005
- Martz, T. R., J. G. Connery, and K. S. Johnson. 2010. Testing the Honeywell Durafet® for seawater pH applications. *Limnol. Oceanogr.: Methods* **8**: 172–184. doi:10.4319/lom.2010.8.172
- Millero, F. J. 1995. Thermodynamics of the carbon-dioxide system in the oceans. *Geochim. Cosmochim. Acta* **59**: 661–677. doi:10.1016/0016-7037(94)00354-O
- Millero, F. J. 2007. The marine inorganic carbon cycle. *Chem. Rev.* **107**: 308–341. doi:10.1021/cr0503557
- Millero, F. J., R. Woosley, B. DiTrollo, and J. Waters. 2009. Effect of ocean acidification on the speciation of metals in seawater. *Oceanography* **22**: 72–85. doi:10.5670/oceanog.2009.98
- Mills, A., Q. Chang, and N. McMurray. 1992. Equilibrium studies on colorimetric plastic film sensors for carbon dioxide. *Anal. Chem.* **64**: 1383–1389. doi:10.1021/ac00037a015
- Mills, A., and L. Monaf. 1996. Thin plastic film colorimetric sensors for carbon dioxide: Effect of plasticizer on response. *Analyst* **121**: 535–540. doi:10.1039/AN9962100535
- Mohrholz, V., M. Naumann, G. Nausch, S. Krüger, and U. Gräwe. 2015. Fresh oxygen for the Baltic Sea — an exceptional saline inflow after a decade of stagnation. *J. Mar. Syst.* **148**: 152–166. doi:10.1016/j.jmarsys.2015.03.005
- Mosley, L. M., S. L. G. Husheer, and K. A. Hunter. 2004. Spectrophotometric pH measurement in estuaries using thymol blue and m-cresol purple. *Mar. Chem.* **91**: 175–186. doi:10.1016/j.marchem.2004.06.008
- Müller, B. J., T. Rappitsch, C. Staudinger, C. Rüschtz, S. M. Borisov, and I. Klimant. 2017. Sodium-selective fluoroionophore-based optodes for seawater salinity measurement. *Anal. Chem.* **89**: 7195–7202. doi:10.1021/acs.analchem.7b01373
- Orr, J. C., and others. 2005. Anthropogenic ocean acidification over the twenty-first century and its impact on calcifying organisms. *Nature* **437**: 681–686. doi:10.1038/nature04095
- Perez de Vargas Sansalvador, I. M., C. D. Fay, J. Cleary, A. M. Nightingale, M. C. Mowlem, and D. Diamond. 2016. Autonomous reagent-based microfluidic pH sensor platform. *Sens. Actuators B Chem.* **225**: 369–376. doi:10.1016/j.snb.2015.11.057
- Pierrot, D. E., D. W. R. Wallace, and E. Lewis. 2011. MS Excel program developed for CO₂ system calculations. Carbon Dioxide Information Analysis Center. doi: 10.3334/CDIAC/otg.CO2SYS_XLS_CDIAC105a
- Rérolle, V. M. C., C. F. A. Floquet, M. C. Mowlem, D. P. Connelly, E. P. Achterberg, and R. R. G. J. Bellerby. 2012. Seawater-pH measurements for ocean-acidification observations. *TrAC Trends Anal. Chem.* **40**: 146–157. doi:10.1016/j.trac.2012.07.016
- Rérolle, V. M. C., C. F. A. Floquet, A. J. K. Harris, M. C. Mowlem, R. R. G. J. Bellerby, and E. P. Achterberg. 2013. Development of a colorimetric microfluidic pH sensor for autonomous seawater measurements. *Anal. Chim. Acta* **786**: 124–131. doi:10.1016/j.aca.2013.05.008
- Roy, R. N., L. N. Roy, K. M. Vogel, C. Porter-Moore, T. Pearson, C. E. Good, F. J. Millero, and D. M. Campbell. 1993. The dissociation constants of carbonic acid in

- seawater at salinities 5 to 45 and temperatures 0 to 45°C. *Mar. Chem.* **44**: 249–267. doi:[10.1016/0304-4203\(93\)90207-5](https://doi.org/10.1016/0304-4203(93)90207-5)
- Schutting, S., S. M. Borisov, and I. Klimant. 2013. Diketo-pyrrolo-pyrrole dyes as new colorimetric and fluorescent pH indicators for optical carbon dioxide sensors. *Anal. Chem.* **85**: 3271–3279. doi:[10.1021/ac303595v](https://doi.org/10.1021/ac303595v)
- Schutting, S., I. Klimant, D. de Beer, and S. M. Borisov. 2014. New highly fluorescent pH indicator for ratiometric RGB imaging of pCO₂. *Methods Appl. Fluoresc.* **2**: 024001. doi:[10.1088/2050-6120/2/2/024001](https://doi.org/10.1088/2050-6120/2/2/024001)
- Schutting, S., T. Jokic, M. Strobl, S. M. Borisov, D. de Beer, and I. Klimant. 2015. NIR optical carbon dioxide sensors based on highly photostable dihydroxy-aza-BODIPY dyes. *J. Mater. Chem. C* **3**: 5474–5483. doi:[10.1039/C5TC00346F](https://doi.org/10.1039/C5TC00346F)
- Severinghaus, J. W., and A. F. Bradley. 1958. Electrodes for blood pO₂ and pCO₂ determination. *J. Appl. Physiol.* **13**: 515–520. doi:[10.1152/jappl.1958.13.3.515](https://doi.org/10.1152/jappl.1958.13.3.515)
- Shitashima, K. 2010. Evolution of compact electrochemical in-situ pH-pCO₂ sensor using ISFET-pH electrode. AGU Full Meeting Abstracts, 1-4. doi: [10.1109/Oceans.2010.5663782](https://doi.org/10.1109/Oceans.2010.5663782)
- Strobl, M., T. Rappitsch, S. M. Borisov, T. Mayr, and I. Klimant. 2015. NIR-emitting aza-BODIPY dyes – new building blocks for broad-range optical pH sensors. *Analyst* **140**: 7150–7153. doi:[10.1039/C5AN01389E](https://doi.org/10.1039/C5AN01389E)
- Sutton, A. J., and others. 2014. A high-frequency atmospheric and seawater pCO₂ data set from 14 open-ocean sites using a moored autonomous system. *Earth Syst. Sci. Data* **6**: 353–366. doi:[10.5194/essd-6-353-2014](https://doi.org/10.5194/essd-6-353-2014)
- Takeshita, Y., T. R. Martz, K. S. Johnson, and A. G. Dickson. 2014. Characterization of an ion sensitive field effect transistor and chloride ion selective electrodes for pH measurements in seawater. *Anal. Chem.* **86**: 11189–11195. doi:[10.1021/ac502631z](https://doi.org/10.1021/ac502631z)
- Xie, X., and E. Bakker. 2013. Non-severinghaus potentiometric dissolved CO₂ sensor with improved characteristics. *Anal. Chem.* **85**: 1332–1336. doi:[10.1021/ac303534v](https://doi.org/10.1021/ac303534v)

Acknowledgments

Financial support from is gratefully acknowledged from the European Commission Seventh Framework Programme SenseOcean (Grant 614141). JDM received funding from the EU BONUS project PINBAL through Grant 03F0689A.

Conflict of Interest

None declared.

Submitted 5 March 2018

Revised 23 May 2018

Accepted 24 May 2018

Associate editor: Mike DeGrandpre